J Therm Anal Calorim (2011) 104:685–691
DOI 10.1007/s10973-010-0986-3

Non-isothermal kinetics of thermal decomposition of $NH_4ZrH(PO_4)_2{\cdot}H_2O$

Wenwei Wu · Xuehang Wu · Shuibin Lai · Sen Liao

Received: 4 June 2010 / Accepted: 26 July 2010 / Published online: 12 August 2010

Abstract Nanocrystalline $NH_4ZrH(PO_4)_2{\cdot}H_2O$ was synthesized by solid-state reaction at low heat using $ZrOCl_2{\cdot}8H_2O$ and $(NH_4)_2HPO_4$ as raw materials. X-ray powder diffraction analysis showed that $NH_4ZrH(PO_4)_2{\cdot}H_2O$ was a layered compound with an interlayer distance of 1.148 nm. The thermal decomposition of $NH_4ZrH(PO_4)_2{\cdot}H_2O$ experienced four steps, which involves the dehydration of the crystal water molecule, deamination, intramolecular dehydration of the protonated phosphate groups, and the formation of orthorhombic ZrP_2O_7. In the DTA curve, the three endothermic peaks and an exothermic peak, respectively, corresponding to the first three steps' mass losses of $NH_4ZrH(PO_4)_2{\cdot}H_2O$ and crystallization of ZrP_2O_7 were observed. Based on Flynn–Wall–Ozawa equation and Kissinger equation, the average values of the activation energies associated with the $NH_4ZrH(PO_4)_2{\cdot}H_2O$ thermal decomposition and crystallization of ZrP_2O_7 were determined to be 56.720 ± 13.1, 106.55 ± 6.28, 129.25 ± 4.32, and 521.90 kJ mol^{-1}, respectively. Dehydration of the crystal water of $NH_4ZrH(PO_4)_2{\cdot}H_2O$ could be due to multi-step reaction mechanisms: deamination of $NH_4ZrH(PO_4)_2$ and intramolecular dehydration of the protonated phosphate groups from $Zr(HPO_4)_2$ are simple reaction mechanisms.

Keywords $NH_4ZrH(PO_4)_2{\cdot}H_2O$ · Non-isothermal kinetics · Thermal decomposition · Solid-state reaction at low heat

W. Wu (✉) · X. Wu · S. Lai · S. Liao
School of Chemistry and Chemical Engineering, Guangxi University, Nanning 530004, China
e-mail: gxuwuwenwei@yahoo.com.cn

Introduction

Polyvalent metal phosphates considerably possess industrial interesting properties nowadays because of their wide applications in highly selective ion exchangers, acid catalysts, protonic conductors, and novel functionalized materials [1–4]. Zirconium phosphates are an important class of polyvalent metal compounds that occur in two basic forms: α- and γ-zirconium phosphates (α-ZrP and γ-ZrP) represented by the formulae $Zr(HPO_4)_2{\cdot}H_2O$ and $Zr(PO_4)(H_2PO_4){\cdot}2H_2O$, respectively. These compounds were first prepared by Clearfield and Stynes [5] using reflux methods. Later, Carrière et al. [6] obtained α-ZrP crystal using sol–gel method. Additional methods of synthesis have been developed. Specifically, Alberti [7] obtained α-ZrP with a high degree of crystallinity by a direct precipitation method—the so-called fluorine complex method. Tarafdar et al. [8] obtained spherical mesostructured zirconium phosphate by direct precipitation method in the presence of tetradecyl trimethylammonium bromide (TTMAB) in alkaline medium when zirconium carbonate complex and $NH_4H_2PO_4$ were used as raw materials. Yamanaka et al. [9] obtained pure phase $MZr_2(PO_4)_3$(M = Na, K) by hydrothermal synthesis method when fluorine ion was used as mineralized agent. Wu et al. [10] obtained pure phase ammonium zirconium phosphates [$NH_4ZrH(PO_4)_2{\cdot}H_2O$] powder via solid-state reaction at low heat when $ZrOCl_2{\cdot}8H_2O$ and $(NH_4)_2HPO_4$ were used as raw materials, and studied its catalytic performance in the synthesis of butyl acetate. The result showed that $NH_4ZrH(PO_4)_2{\cdot}H_2O$ behaved as an excellent heterogeneous catalyst in the synthesis of butyl acetate.

Thermal treatment of inorganic phosphate substances has a great synthetic potential, as it may turn simple compounds into advanced materials, such as ceramics, catalysts, and glasses. The mechanism and kinetics studies of solid-state

reactions are needed to take advantage of this potential [11–13]. In this article, the mechanisms and kinetics of the decomposition of $NH_4ZrH(PO_4)_2{\cdot}H_2O$ were studied using TG–DTA technique. Non-isothermal kinetics of the decomposition process of $NH_4ZrH(PO_4)_2{\cdot}H_2O$ were interpreted by Flynm–Wall–Ozawa (FWO) method [14, 15] and Kissinger method [16].

Experimental

Reagent and apparatus

All the chemicals were of reagent grade purity. TG/DTA measurements were made using a Netsch 40PC thermogravimetric analyzer. X-ray powder diffraction (XRD) was performed using a Rigaku D/max 2500 V diffractometer equipped with a graphite monochromator and a Cu target.

Preparation of nanocrystalline $NH_4ZrH(PO_4)_2{\cdot}H_2O$

The binary ammonium zirconium phosphates $NH_4ZrH(PO_4)_2{\cdot}H_2O$ were prepared by the solid-state reaction at low heat using $ZrOCl_2{\cdot}8H_2O$ and $(NH_4)_2HPO_4$ as starting materials [10]. In a typical procedure, $ZrOCl_2{\cdot}8H_2O$ (5.0 g), $(NH_4)_2HPO_4$ (5.0 g), and surfactant PEG (polyethylene glycol)-400 (1.0 mL) were fully ground in a mortar with a rubbing mallet for 40 min at first, and then the mushy reaction mixture was sealed and heated at 353 K for 2 days after the pH value of reaction mixture was adjusted between 1 and 2 with 50% H_3PO_4. The mixture was washed with deionized water to remove soluble inorganic salts until Cl^- ion could not be visually detected by 0.1 mol L^{-1} $AgNO_3$ solution. The precipitate was then washed with a small amount of anhydrous ethanol and dried at 353 K for 3 h to give the pure phase nanocrystalline $NH_4ZrH(PO_4)_2{\cdot}H_2O$ with layered structure.

Method of determining kinetic parameters

Determination of activation energy by Flynn–Wall–Ozawa method [14, 15]

Kinetic equation of solid-state reaction can be expressed as Eq. 1:

$$\frac{d\alpha}{dt} = Ae^{-E_a/RT}f(\alpha) \tag{1}$$

When heating rate is kept fixed value, that is: $\beta = dT/dt$. Equation 1 can be rewritten into the Eq. 2:

$$\frac{d\alpha}{dT} = \frac{A}{\beta}e^{-E_a/RT}f(\alpha) \tag{2}$$

where E_a is the apparent activation energy, A is the pre-exponential factor, R is the gas constant, and α is called the reaction degree. The $f(\alpha)$ is a function of α, which reveals the mechanism of reaction. By a series of transforms, thus Eq. 2 can thus be rewritten as the Eq. 3:

$$\log \beta = \left[\log\frac{E_aA}{R} - \log\, g(\alpha) - 2.315\right] - 0.4567\frac{E_a}{RT} \tag{3}$$

If α is a fixed value, then $\log g(\alpha)$ is a fixed value, too. The dependence of $\log \beta$ on $1/T$ must give rise to a straight line. Thus, reaction activation energy E_a can be obtained from linear slope ($k = -0.4567E_a/R$).

Determination of activation energy and pre-exponential factor by Kissinger method [16]

According to the DTA curve and the Kissinger equation (Eq. 4), the activation energy and pre-exponential factor of thermal decomposition reaction and ZrP_2O_7 crystallization can be obtained.

$$\ln\frac{\beta}{T_{max}^2} = -\frac{E_a}{RT_{max}} + \ln\frac{AR}{E_a} \tag{4}$$

where β is the heating rate (K min^{-1}), T_{max} is the most rapidly decomposing temperature (that is, peak temperature on DTA curve, K), E_a is the thermal decomposing activation energy (kJ mol^{-1}), R is the gas constant (8.314 J·mol^{-1}·K^{-1}), and A is the pre-exponential factor. The dependence of $\ln(\beta/T_{max}^2)$ on $1/T_{max}$ must give rise to a straight line. Thus, reaction activation energy E_a can be obtained from linear slope ($k = -E_a/R$), and the pre-exponential factor A can be obtained from linear intercept ($h = \ln(AR/E_a)$).

Results and discussion

TG/DTA analysis of the synthetic product

Figure 1 shows the TG/DTA curves of the synthetic product at three different heating rates from ambient temperature to 1297 K, respectively.

The DTA peaks closely correspond to the weight changes observed on the TG curves. The TG/DTA curves show that the thermal decomposition of the synthetic product below 973 K occurs in three well-defined steps. The first step starts at about 323 K, characterized by a broad endothermic DTA peak at about 378 K attributed to the dehydration of $NH_4ZrH(PO_4)_2{\cdot}H_2O$ and the formation of anhydrous $NH_4ZrH(PO_4)_2$. The product is stable up to about 498 K, and then decomposed in the second step. This step shows an

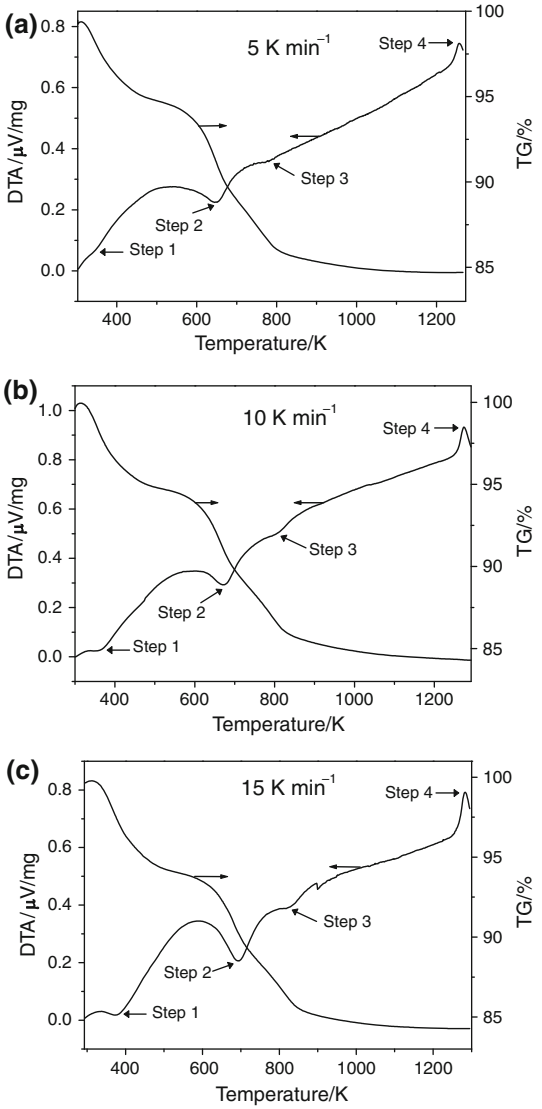

Fig. 1 TG/DTA curves of the $NH_4ZrH(PO_4)_2{\cdot}H_2O$ at different heating rates

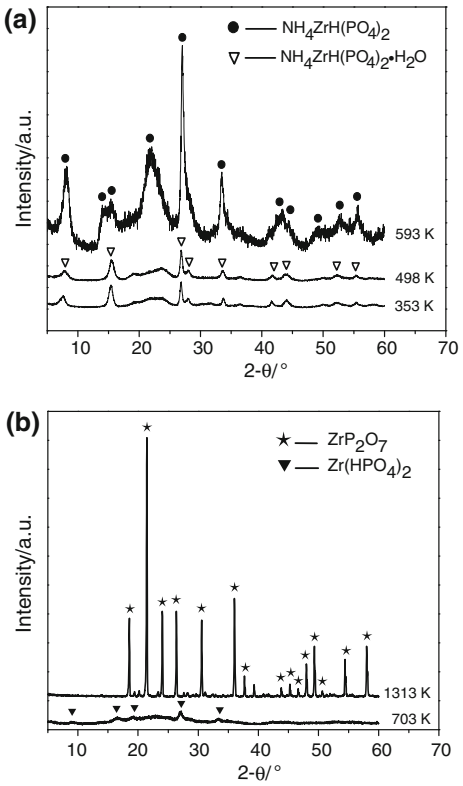

Fig. 2 XRD patterns of the samples obtained at different thermal decomposition temperatures for 3 h

endothermic process with broad DTA peak at about 673 K, which is due to the deamination of $NH_4ZrH(PO_4)_2$ and the formation of $Zr(HPO_4)_2$. The third decomposition step is also endothermic process with DTA peak at about 800 K attributed to the intramolecular dehydration of the protonated phosphate groups from $Zr(HPO_4)_2$, and the formation of amorphous ZrP_2O_7. DTA exothermic peak at about 1273 K is attributed to phase transition from amorphous ZrP_2O_7 to orthorhombic phase ZrP_2O_7.

XRD analysis of the synthetic product and its calcined samples

Figure 2 shows the XRD patterns of the synthetic product dried at 353 K and the products resulting from calcination at different temperatures for 3 h.

From Fig. 2a, all the diffraction peaks from sample obtained at 353 K can be indexed to be in agreement with $NH_4ZrH(PO_4)_2{\cdot}H_2O$, space group *Pbca* (61), from PDF card 52-0351, which shows that the synthetic product is crystalline $NH_4ZrH(PO_4)_2{\cdot}H_2O$. The diffraction peak at about 7.61° for 2θ is attributed to the layered structure of the synthetic product $NH_4ZrH(PO_4)_2{\cdot}H_2O$ with interlayer distance of 1.148 nm; the structure of the $NH_4ZrH(PO_4)_2{\cdot}H_2O$ is stable up to about 498 K, which is in good agreement with that from TG/DTA analysis. When the sample was heated at 593 K for 3 h, the characteristic diffraction peaks of monoclinic $NH_4ZrH(PO_4)_2$ were observed, which is also a layered compound with interlayer distance of 1.1257 nm. From Fig. 2b, the characteristic diffraction peaks of crystalline compound disappeared or became very weak when $NH_4ZrH(PO_4)_2{\cdot}H_2O$ was kept at 703 K for 3 h, suggesting that the structure of the crystalline $NH_4ZrH(PO_4)_2$ was destroyed, and a new amorphous compound had been formed. When the sample was heated at 1313 K for 3 h, strong intensity and smoothed baseline, and a wide- and low-diffraction spectrum of the thermal decomposition product were observed. This indicates that the calcined product has a high degree of crystallinity. All the diffraction peaks in the figure are found to be in agreement with orthorhombic zirconium pyrophosphate (ZrP_2O_7), space group *Pbca* (61),

Table 1 Average particle sizes and lattice parameters of $NH_4ZrH(PO_4)_2{\cdot}H_2O$ and its calcined samples at 593 and 1313 K calculated from XRD data

Compound	Method	*a*/Å	b/Å	c/Å	*β*/°	Average crystallite sizes/nm
$NH_4ZrH(PO_4)_2{\cdot}H_2O$ (353 K)	PDF#52-0351	–	–	–	–	
	This work	–	–	–	–	17 ± 3
	DIF(this work-PDF)	–	–	–	–	
$NH_4ZrH(PO_4)_2$ (593 K)	PDF#82-2401	5.328	6.622	11.326	96.63	
	This work	5.372(0)	6.616(2)	11.363(3)	97.84(2)	18 ± 3
	DIF(this work-PDF)	0.044	−0.006	0.037	1.21	
$Zr(HPO_4)_2$ (703 K)	PDF#21-1494	Non-crystalline				
	This work	Non-crystalline				
	DIF(this work-PDF)	Non-crystalline				
ZrP_2O_7 (1313 K)	PDF#49-1079	8.246	8.246	8.246		
	This work	8.257(0)	8.257(0)	8.257(0)		72 ± 7
	DIF(this work-PDF)	0.011	0.011	0.011		

– Not detectable

from PDF card 73-2296. In contrast to the diffraction pattern of $NH_4ZrH(PO_4)_2{\cdot}H_2O$ or $NH_4ZrH(PO_4)_2$, no diffraction peak at about 7.6° for 2θ of calcined sample from 1313 K for 3 h appears, suggesting that the crystalline ZrP_2O_7 is a non-layered structure compound.

According to the Scherrer formula: $D = K\lambda/(\beta\cos\theta)$, where D is the particle diameter, $K = 0.89$ (Scherrer constant), $\lambda = 0.15406$ nm (wavelength of the X-ray used), β is the width of line at the half-maximum intensity, and θ is the corresponding angle [17]. The resulting particle sizes and lattice parameters of the products obtained at 353, 593, and 1313 K for 3 h are shown in Table 1. From Table 1, the resulting particle sizes of calcined sample at 353 and 593 K have only a little difference. However, the resulting particle size of calcined sample at 1313 K increases rapidly to about 72 nm, which is due to the fact that the former two compounds still keep their layered structure, and that the latter crystalline particles have taken place further growth after polymerization. The lattice parameters of the synthetic product and its calcined samples are in good agreement with those from PDF card of the corresponding compounds.

Activation energy of thermal decomposition of $NH_4ZrH(PO_4)_2{\cdot}H_2O$ and ZrP_2O_7 crystallization process

In accordance with TG/DTA and XRD analyses of the synthetic product and its calcined products mentioned above, thermal decomposition of $NH_4ZrH(PO_4)_2{\cdot}H_2O$ and ZrP_2O_7 crystallization process below 1313 K consist of four steps, which can be expressed as follows:

$$NH_4ZrH(PO_4)_2 \cdot H_2O(cr) \rightarrow NH_4ZrH(PO_4)_2(cr) + H_2O(g) \quad (5)$$

$$NH_4ZrH(PO_4)_2(cr) \rightarrow Zr(HPO_4)_2(am) + NH_3(g) \quad (6)$$

$$Zr(HPO_4)_2(am) \rightarrow ZrP_2O_7(am) + H_2O(g) \quad (7)$$

$$ZrP_2O_7(am) \rightarrow ZrP_2O_7(cr) \quad (8)$$

According to non-isothermal method, the basic data of α and T collected from the TG curves of the thermal decomposition of $NH_4ZrH(PO_4)_2{\cdot}H_2O$ at various heating rates (5, 10, and 15 $K{\cdot}min^{-1}$) are illustrated in Tables 2, 3, and 4 respectively. According to Eq. 3, the plots of log β versus 1000/T corresponding to different conversions α were shown in Fig. 3. It was found that the dependence of log β on $1000/T$ gave rise to a straight line. In accordance with Flynn–Wall–Ozawa equation, the slopes of these straight lines can be determined, then average activation energy for the thermal decomposition step of nanocrystalline $NH_4ZrH(PO_4)_2{\cdot}H_2O$ was obtained. Table 5 shows the

Table 2 Correlative data used for drawing plot of log β versus $1000/T$ for step 1

α	log β					
	0.699	1.000	1.176	0.699	1.000	1.176
	T/K			$1000/T$ K^{-1}		
0.20	329.15	338.75	351.65	3.038	2.952	2.844
0.30	341.15	356.15	362.75	2.931	2.808	2.757
0.40	352.15	365.85	373.65	2.840	2.733	2.676
0.50	363.75	377.15	385.15	2.749	2.651	2.596
0.60	379.15	390.55	398.65	2.637	2.560	2.508
0.70	396.15	409.78	416.26	2.524	2.440	2.402

Table 3 Correlative data used for drawing plot of log β versus 1000/T for step 2

α	log β					
	0.699	1.000	1.176	0.699	1.000	1.176
	T/K			1000/T K^{-1}		
0.2	599.85	617.25	633.76	1.667	1.620	1.578
0.3	618.65	635.25	651.36	1.616	1.574	1.535
0.4	631.65	648.15	665.76	1.583	1.543	1.502
0.5	643.15	659.25	678.00	1.555	1.517	1.475
0.6	652.75	669.85	688.10	1.532	1.493	1.453
0.7	660.30	680.78	697.26	1.514	1.469	1.434

Table 4 Correlative data used for drawing plot of log β versus 1000/T for step 3

α	log β					
	0.699	1.000	1.176	0.699	1.000	1.176
	T/K			1000/T K^{-1}		
0.2	743.65	764.80	784.00	1.345	1.308	1.276
0.3	755.55	779.05	797.15	1.324	1.284	1.254
0.4	767.25	792.85	810.00	1.303	1.261	1.235
0.5	779.35	806.75	821.76	1.283	1.240	1.217
0.6	793.15	823.25	834.46	1.261	1.215	1.198
0.7	805.30	838.28	848.26	1.242	1.193	1.179

activation energy and correlation coefficient (r^2) for the thermal decomposition steps of nanocrystalline $NH_4ZrH(PO_4)_2{\cdot}H_2O$.

Figure 4 shows the Kissinger plots of the synthesized $NH_4ZrH(PO_4)_2{\cdot}H_2O$ sample. From the slopes of the straight lines, the activation energy values of the prepared $NH_4ZrH(PO_4)_2{\cdot}H_2O$ sample in four steps were determined to be 56.81, 102.93, 126.95, and 521.90 kJ mol^{-1}, respectively (Table 6). These activation energies are consistent with the former hypothesis that the intermediate nucleate and crystallize as metastable phase with adequate growth kinetics before the stable phase orthorhombic ZrP_2O_7. The final step exhibits particularly high activation energy value in comparison with the other three steps, which suggests that crystallization of amorphous ZrP_2O_7 has a slower conversion rate.

From Tables 5 and 6, the activation energies calculated by the FWO and the Kissinger methods are close to each other, so that the results are credible. It was considered that the E_a values are independent of α if the relative error of the slope of the FWO equation straight line is lower than 10%. If E_a values are independent of α, then the decomposition may be a simple reaction, while the dependence of E_a on α should be interpreted in terms of multi-step reaction mechanisms [18–22]. From Table 5, the activation energies change of the step 1 with α is higher than 10%, and that of the step 2 and the step 3 with α are lower than 10%, so that we draw a conclusion that the dehydration of the crystal water of $NH_4ZrH(PO_4)_2{\cdot}H_2O$ could be multi-step reaction mechanisms, and deamination of $NH_4ZrH(PO_4)_2$ and intramolecular dehydration of the protonated phosphate groups from $Zr(HPO_4)_2$ are simple reaction mechanisms.

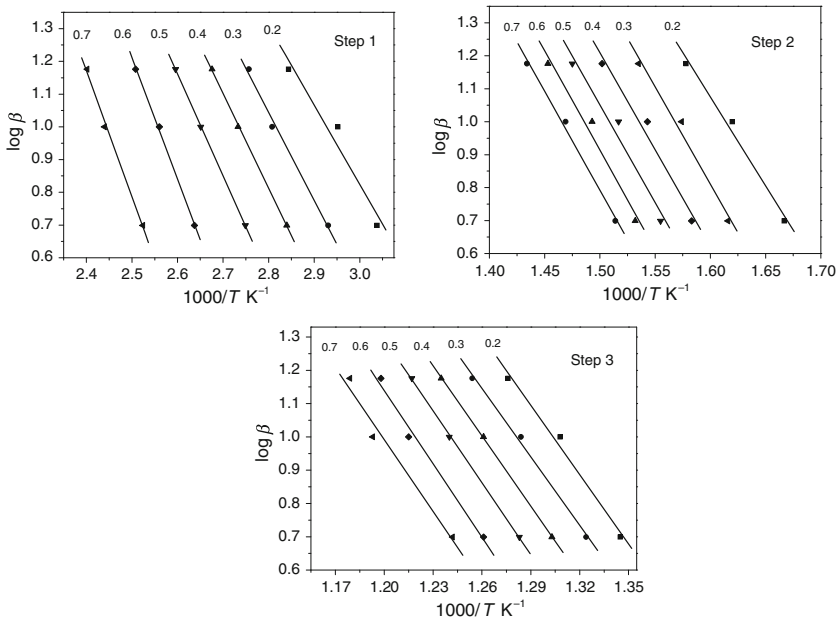

Fig. 3 FWO analysis for the thermal decomposition of $NH_4ZrH(PO_4)_2{\cdot}H_2O$

Table 5 Activation energies ($E\alpha$) and correlation coefficient (r^2) calculated by FWO method

α	Step 1		Step 2		Step 3	
	E_α/kJ mol^{-1}	r^2	E_α/kJ mol^{-1}	r^2	E_α/kJ mol^{-1}	r^2
0.2	44.02	0.9541	97.71	0.9859	126.05	0.9886
0.3	48.76	0.9928	107.30	0.9840	126.41	0.9964
0.4	52.94	0.9995	107.00	0.9765	126.59	0.9995
0.5	56.76	0.9999	108.09	0.9683	130.41	0.9991
0.6	67.60	0.9985	110.27	0.9766	134.70	0.9860
0.7	70.22	0.9959	108.95	0.9948	131.33	0.9749
Av	56.72 ± 13.10	0.9901	106.55 ± 6.28	0.9810	129.25 ± 4.32	0.9908

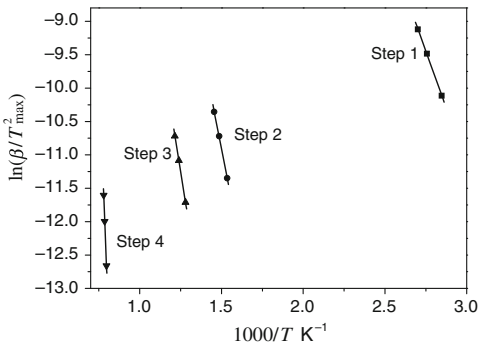

Fig. 4 Kissinger plots of the transformation due to the dehydration (step 1), deamination (step 2), polycondensation (step 3), and crystallization of ZrP_2O_7 (step 4) steps of $NH_4ZrH(PO_4)_2{\cdot}H_2O$

Table 6 Kinetic parameters obtained from Kissinger method

	Step 1	Step 2	Step 3	Step 4
Activation energy E_a/kJ mol^{-1}	56.81	102.93	126.95	521.90
ln A	18.17	17.09	17.47	48.39
r^2	0.9997	0.9993	0.9998	0.9993

Conclusions

When $ZrOCl_2{\cdot}8H_2O$ and $(NH_4)_2HPO_4$ were used as raw materials, pure phase nanocrystalline $NH_4ZrH(PO_4)_2{\cdot}H_2O$ with layered structure was obtained via solid-state reaction at low heat, in which particle size and interlayer distance were 17 ± 3 nm and 1.148 nm, respectively. The thermal decomposition of $NH_4ZrH(PO_4)_2{\cdot}H_2O$ in the range of 299–1313 K is a complex process, which involves the dehydration of the crystal water molecule, deamination, intramolecular dehydration of the protonated phosphate groups, and formation of orthorhombic ZrP_2O_7. The average values of the activation energies associated with the three steps of $NH_4ZrH(PO_4)_2{\cdot}H_2O$ thermal decomposition and crystallization of ZrP_2O_7 were 56.720 ± 13.1, 106.55 ± 6.28, 129.25 ± 4.32, and 521.90 kJ mol^{-1}, respectively. Dehydration of the crystal water of $NH_4ZrH(PO_4)_2{\cdot}H_2O$ could be multi-step reaction mechanisms, and deamination of $NH_4ZrH(PO_4)_2$ and intramolecular dehydration of the protonated phosphate groups from $Zr(HPO_4)_2$ are simple reaction mechanisms.

Acknowledgements This study was financially supported by the Guangxi Natural Scientific Foundation of China (Grant No. 0991108), and the Guangxi Science and Technology Agency Research Item of China (Grant No. 0992001-5).

References

1. Parida KM, Sahu BB, Das DP. A comparative study on textural characterization: cation-exchange and sorption properties of crystalline α-zirconium(IV), tin(IV), and titanium(IV) phosphates. J Colloid Interface Sci. 2004;270:436–45.
2. Costa MCC, Hodson LF, Johnstone RAW, Junyao L, Whittaker D. The mechanism of gas-phase dehydration of cyclohexanol and the methylcyclohexanols catalysed by zirconium phosphate and zirconium phosphite. J Mol Catal A Chem. 1999;142:349–60.
3. Rustum R, Vance ER, Alamo J. [NZP], a new radiophase for ceramic nuclear waste forms. Mater Res Bull. 1982;17:585–9.
4. Krishna RM, Kevan L. Photoinduced electron transfer from *N*,*N*,*N*′,*N*′-tetramethylbenzidine incorporated into layered zirconium phosphate studied by ESR and diffuse reflectance spectroscopies. Micropor Mesopor Mater. 1999;32:169–74.
5. Clearfield A, Stynes JA. The preparation of crystalline zirconium phosphate and some observations on its ion exchange behaviour. J Inorg Nucl Chem. 1964;26:117–29.
6. Carrière D, Moreau M, Lhalil K, Barboux P, Boilot JP. Proton conductivity of colloidal nanometric zirconium phosphates. Solid State Ionics. 2003;162–163:185–90.
7. Alberti G. Syntheses, crystalline structure and ion-exchange properties of insoluble acid salts of tetravalent metals and their salt forms. Acc Chem Res. 1978;11:163–70.
8. Tarafdar A, Panda AB, Pradhan NC, Pramanik P. Synthesis of spherical mesostructured zirconium phosphate with acidic properties. Micropor Mesopor Mater. 2006;95:360–5.
9. Yamanaka S, Yoshioka K, Hattori M. Unusual ionic conductivities of hydrothermally prepared $MZr_2(PO_4)_3$ (M = Na, K). Solid State Ionics. 1990;40–41:43–7.
10. Wu WW, Lai SB, Wu XH, Liao S, Hou SY. Preparation of $NH_4ZrH(PO_4)_2\ H_2O$ via solid-state reaction at low heat and study on catalytic synthesis of butyl acetate. Rare met. 2008;27:550–4.
11. Logvinenko V. Solid state coordination chemistry. The quantitative thermoanalytical study of thermal dissociation reactions. J Therm Anal Calorim. 2000;60:9–15.

12. Danvirutai C, Noisong P, Youngme S. Some thermodynamic functions and kinetics of thermal decomposition of NH_4MnPO_4 H_2O in nitrogen atmosphere. J Therm Anal Calorim. 2010;100:117–24.
13. Boonchom B. Kinetic and thermodynamic studies of $MgHPO_4$ $3H_2O$ by non-isothermal decomposition data. J Therm Anal Calorim. 2009;98:863–71.
14. Flynn JH, Wall LA. A quick direct method for the determination of activation energy from thermogravimetric data. Polym Lett. 1966;4:323–8.
15. Ozawa TA. New method of analyzing thermogravimetric data. Bull Chem Soc Jpn. 1965;38:1881–6.
16. Kissinger HE. Reaction kinetics in differential thermal analysis. Anal Chem. 1957;29:1702–6.
17. Wu XH, Wu WW, Liao S, Fan YJ, Li SS. Preparation via solid-state reaction at room temperature and characterization of layered nanocrystalline $KMnPO_4$ H_2O. J Alloys Compd. 2009;479:541–4.
18. Vlaev L, Nedelchev N, Gyurova K, Zagorcheva M. A comparative study of non-isothermal kinetics of decomposition of calcium oxalate monohydrate. J Anal Appl Pyrolysis. 2008;81:253–62.
19. Gabal MA. Non-isothermal decomposition of NiC_2O_4–FeC_2O_4 mixture aiming at the production of $NiFe_2O_4$. J Phys Chem Solids. 2003;64:1375–85.
20. Genieva SD, Vlaev LT, Atanassov AN. Study of the thermo-oxidative degradation kinetics of poly(tetrafluoroethene) using iso-conversional calculation procedure. J Therm Anal Calorim. 2010;99:551–61.
21. Budrugeac P, Muşat V, Segal E. Non-isothermal kinetic study on the decomposition of Zn acetate-based sol-gel precursor. J Therm Anal Calorim. 2007;88:699–702.
22. Boonchom B, Danvirutai C. Kinetics and thermodynamics of thermal decomposition of synthetic $AlPO_4$ $2H_2O$. J Therm Anal Calorim. 2009;98:771–7.